Chapter 5

THE ENVIRONMENTAL HYDRAULICS OF TURBULENT BOUNDARY LAYERS

ROBERT J. SCHINDLER and JOSEF DANIEL ACKERMAN

Physical Ecology Laboratory, Department of Integrative Biology,

University of Guelph, Guelph, Ontario, Canada

Turbulent flow over rough boundaries is a common occurrence in nature and the subject of much interest in a range of disciplines. It has long been recognized that the geometry of the boundary (or surface) dictates the flow and turbulence structure on a mean and instantaneous time scale. However, the mechanisms linking flow characteristics to roughness geometry remain poorly quantified, which has implications for our understanding of a variety of processes, particularly those occurring in the near-boundary region. It has been demonstrated that temporal and spatial variations in flow structure are sensitive to a range of geometric parameters describing the boundary geometry. We review the experimental evidence for rough boundary/flow interactions across different disciplines. A synthesis reveals that (1) different approaches have led to the adoption of a variety of parameters that are used to describe boundary roughness, and (2) that different criteria are used to evaluate the relative effects of boundary roughness. Moreover, (3) much of the experimental data relates to idealized surfaces that do not reflect the complexity of natural boundaries, or (4) is taken in low Reynolds number flows, and generally cannot be applied to aquatic flows in nature. The implications for our understanding of near-bed aquatic processes in turbulent boundary layers are discussed, and suggestions for future research approaches are presented.

1.0 Introduction

Unidirectional turbulent flow over rough boundaries (or surfaces) is a common occurrence in nature and the subject of much interest in a range of disciplines that can classified under the rubric of environmental hydraulics. One of the best models of this phenomenon is given by flow over a flat plate [40]. This model provides an ideal or theoretical condition on which to study hydraulic flows in the laboratory and field, and reasonable framework to contrast with nature.

Schindler, R.J. and J.D. Ackerman. 2010. The environmental hydraulics of turbulent boundary layers. pp 87-126 In: D.T. Mihailovic and C. Gualtieri (eds.) *Advances in Environmental Fluid Mechanics*. World Scientific, London. 348 pp.

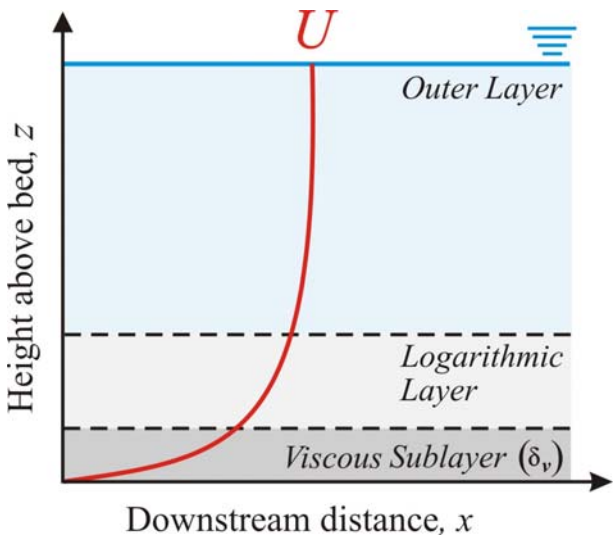

Figure 1. Boundary layer vertical structure with the $\partial u/\partial z$ indicated by the solid line.

The basic concept is that fluids cannot usually penetrate a boundary and this leads to a velocity gradient ($\partial u/\partial z$, where u is the velocity in the x, or downstream, direction and z is the height) perpendicular to the boundary, which increases outward to the free stream velocity (U_0). The region of reduced flow (i.e., < 0.99 U_0) is arbitrarily referred to as the boundary layer, which has a thickness δ, and is a function of the Reynolds number, $Re = lu/\nu$ (where l is a length scale and ν is the kinematic viscosity) and x, in the case of a flat plate. Close to the surface, the boundary layer will become turbulent when the local Re ($Re_x = ux/\nu$) approaches a critical value of 3 to 5 x 10^5, in the case of a flat plate oriented parallel to the flow. In nature this transition is accelerated by the presence of roughness or obstacles on the boundary [40]. The vertical structure is also important in a fully developed boundary layer: (1) The layer adjacent to the boundary is referred to as the viscous sublayer ($\delta_v \approx 10\nu/u_*$, where u_* is the friction velocity, a scale related to $\partial u/\partial z$ near the boundary) in which viscous forces dominate. The viscous sublayer includes a thin diffusional sublayer immediately adjacent to the boundary ($\delta_D \approx \nu/u_*(\nu/D)^{-1/3}$, where D is the molecular diffusivity) [33] where diffusive processes dominates. (2) The next layer is the inertial sublayer or log layer ($\delta_l \approx 0.15\ \delta$), which is a region of rapidly increasing velocity where inertial forces dominate. (3) The outer layer of the boundary layer represents a transition to the free stream flow (Figure 1).

Given that the boundary layers concept is based on spatial and velocity scales it should not be surprising to find that they can be embedded in one another, i.e., there may be a series of boundary layers of increasing sizes defined for (1) a larval mayfly on (2) a pebble in (3) a pebble cluster, on (4) the streambed [6]. Boundary layer flow is not isolated from upstream or downstream obstructions, nor is the flow necessarily uniform over them [19]. Lastly, boundary layers can also be generated by other types of water motion (e.g., wave current boundary layers).

The velocity within a boundary layer can be modeled mathematically using *the law of the wall*, which is a representation of the aforementioned vertical structure. Specifically, the velocity (u) is given as a function of the height (z) given by

$$u = \frac{u_*}{\kappa} \ln\left(\frac{z}{z_0}\right) \tag{1}$$

where $\kappa = 0.4$ is the von Kármán constant, and z_0 is the roughness height. This model allows for the modeling of many flow conditions and also for the estimation of parameter values from data. For example, u_* is equal to κ multiplied by the slope of the linear regression of u on the natural logarithm of z in the log layer, and z_0 is equal to the base of the natural logarithm (e) raised to the value of the y intercept of the same regression [3] (Figure 2). Such estimates provide the ability to quantify the boundary, bed or wall shear stress (τ_w), which is the quotient of the shearing force and the area of the boundary, i.e., $\tau_w = \rho u_*^2$. Indeed, much of the challenge associated with environmental hydraulics has been to model flows and estimate parameters under non-ideal conditions that exist due to a number of factors especially bed roughness. These issues are the subject of this chapter, which focuses on flowing or lotic systems (i.e., rivers and streams).

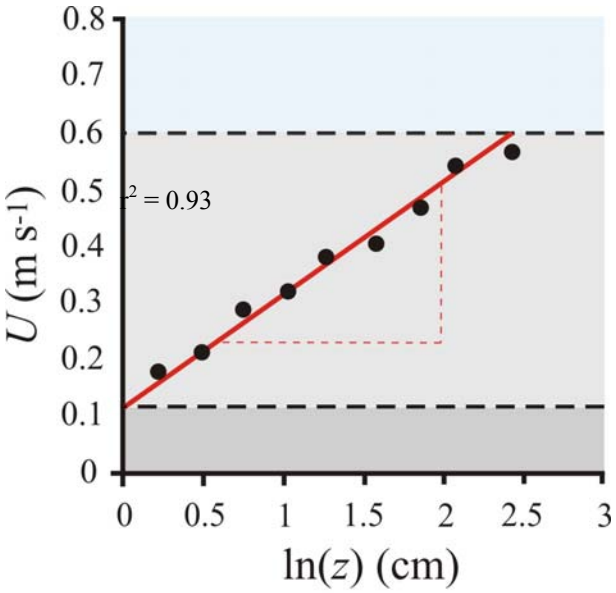

Figure 2. Law of the wall ($u_* = 0.068$ ms^{-1}, $z_o = 0.37\ 10^{-2}$ m, $\tau_w = 4.46$ Pa)

2.0 Understanding Boundary Roughness

In river channels, the boundary layer typically extends to the water surface due to relatively small ratio of flow depth (d) to roughness height (k) (i.e., d/k or relative roughness). The velocity characteristics of fluvial boundary layers have been extensively studied (e.g., [7] [9] [31] [2]). The shape of the downstream velocity profile, the velocity gradient, the turbulent flow characteristics and their links to sediment transport and bedforms have been common research themes in past decades [38].

A basic distinction can be made between the log-layer and outer region in a hydrodynamically rough turbulent boundary layer. The majority of boundary layer research has focused on uniform boundary roughness, or the identification of a common equivalent roughness height, k_s, which represent a spatial averaging of the roughness. The flow is said to be hydrodynamically rough when $k_s > 5\delta_v$ (i.e., the roughness element extends above the viscous sublayer; see below). This condition is met in most rivers, and other fully turbulent flows, where vortices generated around individual roughness elements or impinging from the log layer permanently disrupt the laminar sublayer [38]. These concepts can be integrated

into the law of the wall for straight uniform channels with uniform bed material using the displacement height (d_0,)

$$u = \frac{u_*}{\kappa} \ln\left(\frac{z - d_0}{z_0}\right) \tag{2a}$$

or by using an equivalent roughness height (k_s) [38] given by

$$u = \frac{u_*}{\kappa} \ln\left(\frac{d}{k_s}\right) + 2.40 \tag{2b}$$

when the roughness height is uniform, e.g., $k_s = 30.1 z_0$ (see Figure 3).

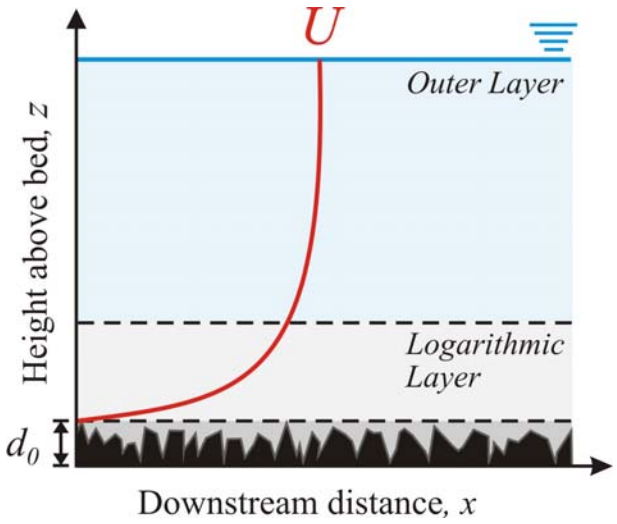

Figure 3. Law of the wall over boundary with uniform roughness.

However, where the roughness is not of uniform height, significant spatial variations in velocity profiles and associated parameters exist. Despite this, eqn. (1) and (2) have been applied to channels with heterogeneous bed material and/or bedforms. k_s can be considered a spatial average of effective roughness height. Numerous studies have shown that k_s is much greater than the median grain size, D_{50} (where the subscript represents the percentile of the grain size range), due to the disproportional effects of larger roughness elements on retarding the flow (e.g., [7]). Typical coefficients are $k_s = 6.8\ D_{50}$ and $k_s = 3.5\ D_{84}$ [9].

Engineering and physical sciences approached tend to model roughness using additional parameters to modify the law of the wall over a smooth bed. A non-dimensional form of the law of the wall is given by

$$u^+ = \frac{1}{\kappa}\ln(z^+) + B \tag{3}$$

where the subscript $^+$ denotes a dimensionless parameter and B is the smooth-wall log-law intercept equal to 5.60 [28]. According to [8] [18] the effects of surface roughness in the roughness layer (see section 3.1) cause a downward shift in the log-law relationship, which they described using a roughness function, Δu^+, given by

$$u^+ = \frac{1}{\kappa}\ln(z^+) + B - \Delta u^+ \tag{4}$$

More recent research has demonstrated that the shift is due to greater momentum absorption over rougher surfaces (see section 3.0). Eqn. (4) can be extended to include the outer layer using the wake function, ω, which provides a 'law of the wake' defined as

$$u^+ = \frac{1}{\kappa}\ln(z^+) + B - \Delta u^+ + \frac{\Pi}{\kappa}\omega\left(\frac{z}{\delta}\right) \tag{5}$$

where Π is dimensionless wake strength. The incorporation of the surface velocity (u_s) in the velocity-defect law provides a means of unifying the overlap between inner and outer regions

$$\left(\frac{u_s}{u_*}\right) - u^+ = -\frac{1}{\kappa}\ln(z/\delta) + B - \Delta u^+ + \frac{\Pi}{\kappa}\omega\left(\frac{z}{\delta}\right). \tag{6}$$

Some studies have reported that Π is greater for rough-wall flows [22]. This implies that accounting for roughness effects on the mean flow through Δu^+ may be limited. Conversely, there is evidence for a universal velocity-defect profile for smooth and rough walls [8] [18].

2.1 Defining Boundary Roughness

In the simplest terms, roughness can be thought of as any deviation from an idealized form such as a flat plate described above. In nature, roughness is

caused by biotic (e.g., periphyton, aquatic larvae) and abiotic features (e.g., substrate, bedforms) on the boundaries. The physical characteristics of natural roughness include the roughness height (k), density, and spacing (wavelength λ, groove width, j, downstream length, l), and their effects on the flow, which are critical issues to consider in environmental hydraulics (Figure 4). For example, the flow over an array of roughness types (sand, variously sized and spaced hemispheres, spheres, and fences) indicated that different boundary roughness geometries may have similar effects on velocity profiles, even though the mechanisms of turbulence generation, mixing and dissipation may differ [40]. This was based on a surface density parameter (total projected frontal area of roughness per unit wall-parallel projected area), which demonstrated that the effect of roughness increased with the density parameter to a critical value after which the mutual sheltering of roughness elements led to a decrease in the effect

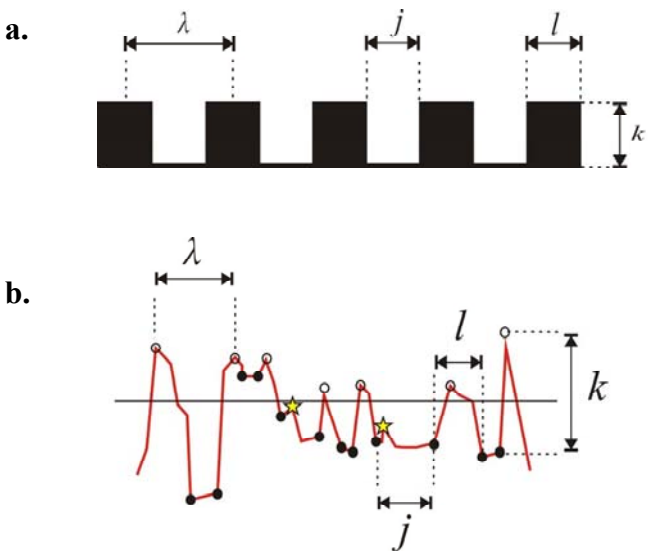

Figure 4. Physical descriptions of (a) idealized roughness elements characterized by blocks and (b) natural roughness elements in a bed profile. Each roughness element can be described by its height (k), length in the downstream direction (l), spacing with respect to other elements (λ), and groove width between elements (j). Legend: solid dots = troughs within a profile; hollow dots = peaks within a profile; and stars = insignificant peaks (i.e., below threshold indicated by solid line) within a profile.

of roughness. That analysis was somewhat limited because it did not fully characterize the surface, and correlations may be to limited to particular experiments. Consequently, most attempts to examine the relationship between roughness and flow characteristics are restricted to surfaces whose geometry is easily described [21]. Studies of flow over these idealized objects have been successful in elucidating the effects of relative size, spacing, arrangement and two-dimensional (2D) or three-dimensional (3D) roughness configuration upon flow resistance, turbulence generation and dissipation (see below).

Three types of flow-roughness interactions were defined by [29] based on the premise that resistance was primarily a function of energy extraction due to the formation of turbulent wakes around individual roughness elements. Using elements of equal height, length and width, but differently spaced in x, [29] identified: (i) *Isolated roughness flow*, where the coherent structure generated by the wake of an upstream element is dissipated before the next element downstream; (ii) *Skimming flow*, where the elements are sufficiently close to prevent the spaces between elements being filled with low-velocity water; and (iii) *Wake interference flow* marking the transition between (i) and (ii), where the wake structures of successive elements impinge on one another to generate additional turbulence. A fourth type was included by [10] (iv) *Chaotic flow* in shallow rough flows where $d < 3k$ (Figure 5). This conceptual framework was an attempt to categorize flow conditions via roughness parameters such as k, λ, l, and j.

The importance of the connectivity of the fluid between roughness elements and the fluid above the roughness elements underlies the distinction that has been made between (1) k-type roughness, where k_s is proportional to k and (2) d-type roughness, where k_s is proportional to δ rather than k [35]. The usual explanation is that d-type roughness sustains stable recirculation (or vortices) that isolate the fluid between the roughness from the outer flow. The effective length scale determining k_s is not k, but $k - d$ (or the 'error-in-origin'; [35]). Where the distance between the edges of elements, or groove width (j), is wider than 3 - 4k, the recirculation zone reattaches before the next roughness element, exposing it to the outer flow. The thresholds between each flow type are dictated by k, and the downstream distance between roughness elements given by λ, j, and l (e.g., [29] [34] [10] [44] [21]). Ratios of these length scales have been used to develop a number of dimensionless parameters that are used to describe bed roughness geometry (Table 1).

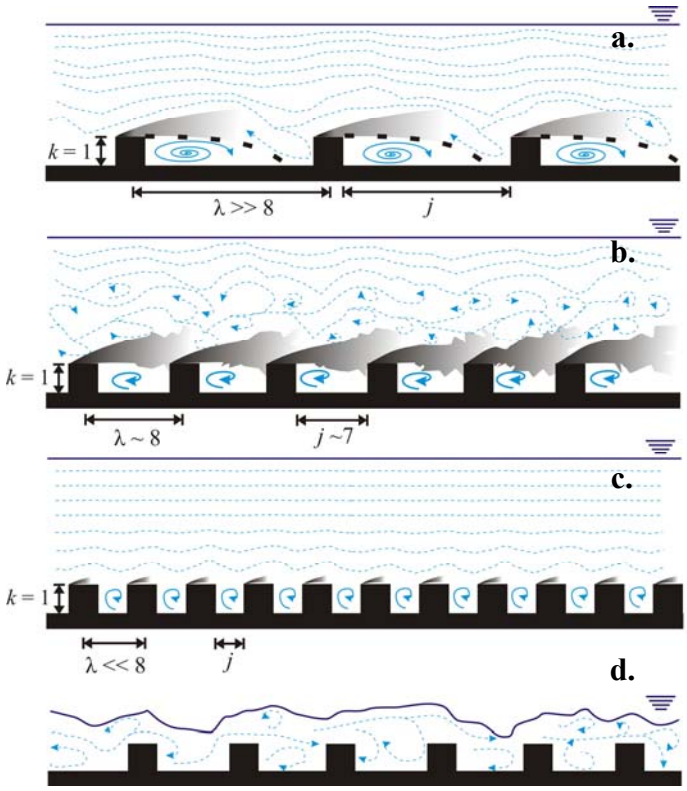

Figure 5. Hydrodynamic regimes defined by flow-roughness interactions include (a) isolated roughness flow, (b) wake interference flow (c) skimming flow, and (d) chaotic flow. Regimes are defined by water depth k, λ, and j (after [29] [10]).

For high Reynolds numbers ($Re = Ud/\nu$), the threshold roughness spacing, $\lambda_{Crit,}$ between isolated roughness flow and wake interference flow is given by

$$\frac{\lambda / k}{C_D(1 - nj / P)} = 67.2 / \left(\frac{100}{(2\log(d / \lambda) + 1.75)^2} \right) \qquad (7)$$

where C_D is drag coefficient, n is the number of elements in a cross-section, P is wetted perimeter and d is flow depth [29]. The term nj/P represents the proportion of the flat surface between the roughness elements, and $C_D\ (1- nj/P)$ varied with roughness density. When roughness density was constant, the critical

value λ_{Crit} varied with k and d, but [44] showed λ_{Crit} increased with d according to

$$\lambda_{Crit} = 2.46k\left(\frac{d}{k}\right)^{0.42} \quad (8)$$

Note that eqn. (8) is limited because it is based on a single value of C_D (1- *ns/P*) and assumes long, flat roughness elements.

Table 1: Summary of bed geometry parameters derived from experiments over idealized objects.

Parameter	*Ratio*	*Reference*
Roughness Index	λ/k	[29]
Relative Roughness Spacing	k/λ	[29]
Roughness Spacing Index	λ/j	[29]
Dimensionless Groove Width	j/k	[44]
Blockage Ratio	δ/k, $\delta = d$ in most natural channels	[21]

2.2 Parameterizing Boundary Roughness

The threshold between skimming flow and wake interference flow is relevant as it represents a transition from a bed characterized by sheltered zones of separated flow between elements to that perturbed by turbulent structures. Physically, the threshold is defined as the point where $j > k$. The turbulent wake occupies the entire grove width and is stable, i.e., skimming flow. When $j > k$, the wake will is increasingly unstable in a manner common to flow separation in the lee of obstacles, leading to wake interference flow [44].

The exact ratio j/k that defines the threshold between each state is a function of the shape of the roughness elements (see section 3.3.5). More importantly, for a coarse clastic river bed the variables λ, j and k are not easily determined. Initially, a "significant roughness element" must be chosen arbitrarily. For instance, a small element below the average roughness height may be considered significant if exposed, and may exert more flow resistance than a much larger element sheltered by a close neighbour. A visual interpretation of the roughness

profile in cobble-bed rivers was used in [44] to determine λ. It was estimated that k was equivalent to two times the average deviation away from the height, and the groove width (j) approximated the roughness spacing minus the D_{50} of the long axis on the basis that cobbles generally lie with their short axes vertical and their long axes aligned to the flow. This provided a value of $j/k = 1.0$ for 'stream bed roughness'.

The 'average' flow condition in nature appears to be wake interference [44]. Using high spatial resolution profiles of downstream velocity and visual observations in modelled cobble beds in flume channels, [44] isolated all three flow states, plus chaotic flow around a relatively large obstacle ($d < 3k$). The term $C_D\ (1- ns/P)$ ranged from 0.4 - 0.8 and the dominant condition was wake interference flow, validating the approach. It is evident that the choice of criteria for the selection of significant roughness element can have a profound affect on the outcome. For example, Figure 6a presents a bed profile taken at 2.5 cm increments with a 1 mm vertical resolution in mid channel in a cobble bed stream in southern Ontario. The selection of significant roughness elements using objective criteria such as relative depths (k/d) of 10, 30 or 50 led to dramatically different outcomes in terms of the interpretation of the parameters used to describe the roughness (e.g., k) from the same dataset (Figure 6b; Schindler and Ackerman, unpublished). Whereas this approach is somewhat subjective, the results are intriguing and warrant further study for application across a range of bed morphologies (see section 3.3.3).

2.3 Determining the Spatial Complexity of Boundary Roughness

Given the complexity of channel bed topography, it is not surprising that a single, universal parameter to describe the effects of boundary roughness on flow and turbulence structure has been sought [42]. Because of the simplicity of relating downstream velocity profile characteristics to k_s or D_x, this approach is often used in environmental hydraulics. However, this is a somewhat of a 'black box' approach because it neglects variations in bed structure [7] [9] [31] [2].

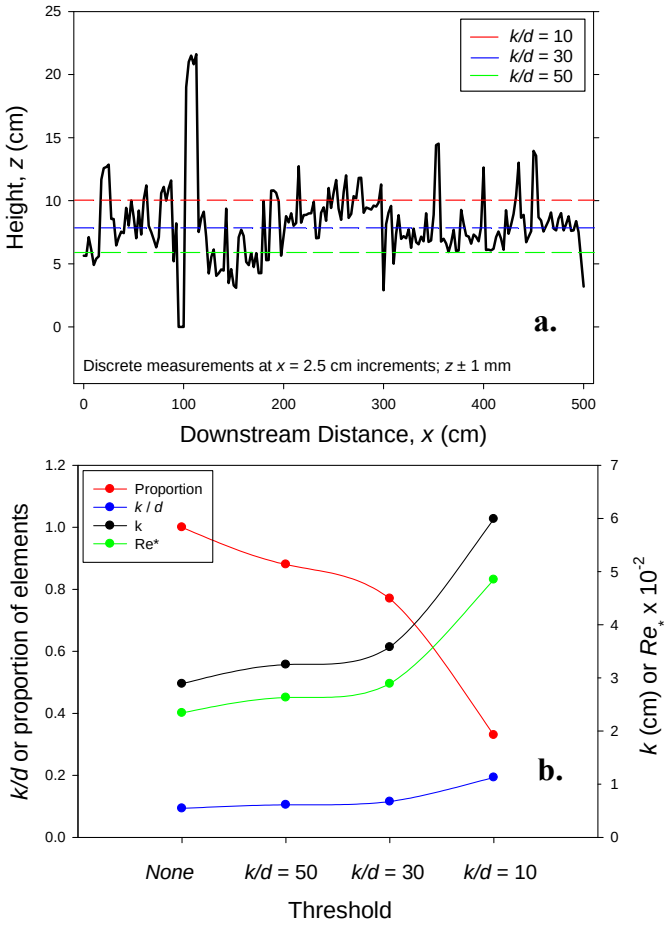

Figure 6. The effect of the threshold selection on roughness parameters. (a) a bed profile in mid channel in a cobble bed stream, and (b) the effect of different thresholds on roughness parameters (Schindler and Ackerman, unpublished).

Apparently, bed structure (particle shape, orientation, height variation, degree of packing, structural arrangement) may significantly affect the overall hydraulic resistance because turbulent structures generated at the boundary are ultimately responsible for the extraction of mean flow energy, i.e., resistance [31]. In other words, the use of D_x as a roughness parameter requires that independently formed roughness surfaces with the same value of D_x show exactly the same resistance to

flow for identical hydraulic conditions [1]. The size, intensity and longevity of turbulent structures governing the mean flow field are, therefore, a product of (1) the geometry of the roughness obstacle and (2) flow conditions (assuming the absence of bedforms).

2.3.1 Statistical Measures of Boundary Roughness

Various statistical measures of bed roughness have been suggested. For example, the difference between the highest point on the particle and the average elevation of the points of contact with adjacent particles could be used for the effective roughness height. The evaluation given by [11] of percentile grain sizes supported the use of K_3, which is the maximum difference between three adjacent points on a bed profile. This statistical approach is limited, as it depends on the sampling interval used [31], and [43] showed that k_s was dependent on the density of roughness elements, and $k_s = 3D_{84}$ even when the flow deviated significantly from a vertical logarithmic profile.

Another method uses the statistical moments of the distribution of discrete measurements of z to describe the roughness surface. It was shown by [2] that gravel-bed channels exhibiting a step-pool morphology or exhibiting high gradients were better described by the standard deviation of bed elevations (σ^2_z) than by D_x. Conversely, [1] found that σ^2_z was closely related to changes in D_{50} and D_{84}. The skewness of the distribution also increased with the level of armoring, which reflects the settling of finer particles, ultimately reducing the magnitude of surface elevations below mean bed height.

2.3.2 Random Field Approach to Characterizing Boundary Roughness

An alternative way of accounting for bed surface geometry is to describe the roughness as a random field of surface elevations in the downstream and transverse directions $z(x,y)$ (e.g., [31] [2]). This method is popular due to technological advances (e.g., laser scanning) that have facilitated the detailed measurement of bed surfaces.

Random roughness has also been characterized using second-order structure functions that investigate the scaling properties of various rough surfaces [31]. This approach is equivalent to semivariograms used by [9] to describe gravel bed surfaces. The second-order structure function $D(\Delta x, \Delta y)$ of bed elevation $z(x,y)$ is defined as an average square increment

$$\left\{z(x+\Delta x, y+\Delta y)-z(x,y)\right\}^2, \qquad (9)$$

which describes the 'average variance' of the z surface in downstream $(D(\Delta x, \Delta y=0))$ and transverse $(D(\Delta x=0, \Delta y))$ directions based on different spatial sampling lags. The resulting curves of D vs. lag show that at sufficiently large lags, D becomes constant and approximates $2\sigma^2_z$, known as the region of saturation. Small lags corresponds to a scaling region, which can be approximated by a power function i.e., $D(\Delta x) \propto \Delta x^{2H_x}$, where H_x is the scaling exponent. Whereas D provides information on the 'average' surface properties, H_x or H_y (in the transverse direction) can be considered a measure of the complexity of the surface topography (a larger H indicates a smoother profile [5]).

These concepts suggest that statistical moments and the 'random field' approach provide deeper insight into the geometry and surface-forming processes of gravel-bed rivers than a simple characteristic grain size. However, it should be noted that: (1) the concepts have yet to be examined in channels exhibiting smaller or larger ranges in grain size; (2) the application of statistical moments assumes that the distribution of z is Gaussian or near-Gaussian; and (3) the concept is descriptive rather than mechanistic. Detailed comparison of the turbulence field and statistical parameters is required before this approach can be used to understand the role of bed geometry in modifying boundary layer structure and associated turbulent dissipation.

3.0 Hydrodynamics of Rough Boundaries

The aims of this section are: (1) to highlight the differences between near-bed turbulence over smooth- and rough-beds; (2) to elucidate the key geometrical or dimensional parameters describing bed geometry that ultimately dictate near-bed flow and turbulence modification; and (3) to examine the effect of different roughness types (e.g., 2D and 3D surfaces) on the modification of near-bed flow structure.

3.1 Outer Flow Region vs. the Roughness Layer

It is apparent that the ability to describe the flow region at and immediately above roughness elements should provide important insight into their interaction with flow. It would then be possible to expand the description of the vertical structure of a boundary layer over an impermeable rough bed with sufficient depth to include: (1) the interfacial sublayer, δ_t, within the groove space (j) between roughness crests and troughs; (2) the form-induced sublayer, δ_f, in the immediate vicinity of the roughness elements; (3) the logarithmic layer in the flow above the bed; and (4) the outer region [32]. The interfacial sublayer and the form-induced sublayer comprise the roughnesss layer, δ_r, which is subject to turbulent motions that are directly influenced by the roughness characteristics. Its upper-boundary is defined by z_r (Figure 7).

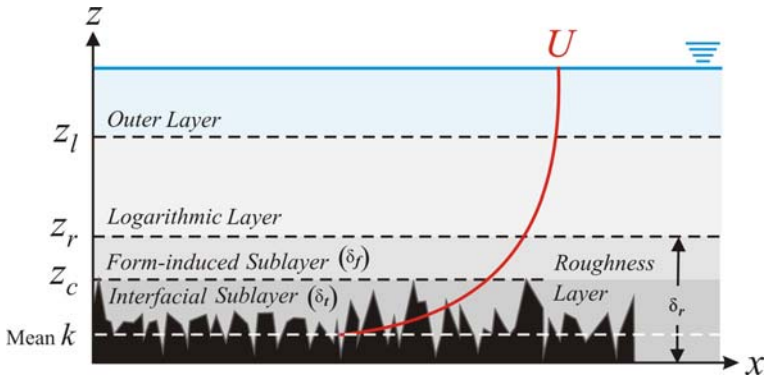

Figure 7. Rough turbulent boundary layers defined using the roughness layer, which is composed of the form-induced and interfacial sublavers.

An important driver of the recent interest in rough boundary flows is the 'similarity hypothesis', which states that at high *Re*, turbulent motions become independent of wall roughness and viscosity at a certain height away from the boundary. This notion can be considered an extension of the Reynolds-number similarity hypothesis for turbulent flows. The theory dictates that smooth and rough walls will exhibit the same turbulence structure in the outer layer, which is a region of weak shear and, therefore, not the site of the dominant instability mechanisms that generate the turbulence, nor of the strongest production of turbulent kinetic energy. Typically, profiles of second-order velocity moments will collapse to common curves in the outer-layer, regardless of wall roughness characteristics [21]. Several experiments have provided substantial support for

the similarity hypothesis (e.g., [4] [17] [37]). Other experiments have shown that the outer flow can exhibit significant structural differences due to the influence of large-scale (e.g., [12] [22] [23]) and small-scale ([42]) coherent turbulent structures specific to individual roughness geometries.

The emphasis on the roughness layer and the validity of the similarity hypothesis also provides an opportunity to elucidate the effects of a large range of bed roughness types and flow conditions. The height to which the roughness layer extends, z_r, is generally considered to be 2 - 5k [23] [37] [21], although [4] suggest that it may be as high as 8k. The range varied with each type of boundary because the turbulent structures that dictate z_r are controlled by different length scales across different surfaces [37]. z_r can be determined in several ways and its thickness is somewhat dependent on the methodology used for parameter selection [4]: (1) the position of the maximum Reynolds shear stress, used to define the upper boundary in shallow flow over rough beds, which is often ill-defined, leading to some uncertainty [36]; and (2) profiles of the variance or standard deviation of a flow parameter can be used to isolate the height at which the parameter reduces to a suitable threshold defined from previous measurements or through physical arguments.

3.2 Key Parameters Dictating Characteristics of the Roughness Layer

3.2.1 Geometrical Parameters

The height of the roughness layer, and the characteristics of turbulence generated within it, varies with changes to the boundary roughness characteristics. The most important roughness parameters are roughness height, k, and spacing, λ, both of which should be considered in terms of relative roughness height (k/d) and roughness index (λ/d). As discussed above, the roughness index dictates the degree to which turbulent structures formed around individual elements interact. The relative roughness height dictates the degree to which elements interact with the entire water depth. Consequently, the shape of the roughness elements, in particular the degree of angularity with respect to the flow (i.e., degree of bluntness), must also be considered (see section 3.3.5).

A distinction can be made between 2D and 3D surfaces, although the bias has been towards 2D geometries due to the ease of measurement in the roughness layer, and in particular the interfacial sublayer. 2D surfaces are almost

exclusively comprised of bars or rods oriented in the transverse direction across channels, and are generally termed *2D transverse bars*. Compared with 2D transverse bars, much less is known about the influence of length scales for 3D roughness [37], due primarily to the inherent complexity of 3D surfaces. The variety of 3D roughness surfaces studied is considerable, and each will exhibit different turbulent characteristics in the roughness layer.

3.2.2 Key Flow Parameters

One effect of wall roughness is the injection of turbulent energy into the flow field. The roughness Reynolds number (Re_*) provides an indication of the influence of the roughness surface on the buffer zone between the inner logarithmic region and the outer flow region in terms of the balance of viscous and form drag forces. It incorporates the height of the roughness surface, k, to describe the influence of the roughness in the boundary layer flow [10]

$$Re_* = u_* k/\nu \qquad (10)$$

Values typically range from 1 x 10^2 to 1 x 10^3 for zero-pressure gradient boundary layer flows. There is little consensus on how to calculate the threshold between hydrodynamically smooth and hydrodynamically rough flows, principally because the use of k neglects the effects of other geometrical parameters, although as mentioned above, $k_s > 5\delta_v$ has been used. For example, [27] found that the roughness types and uniformity dictated the threshold values. Their rough surface, consisting of uniform close-packed spheres, displayed a narrow transitionally-rough regime with $Re_{*smooth} \approx 15$ and $Re_{*rough} \approx 55$. Less uniform close-packed sand grains had a wider transitionally rough regime where $Re_{*smooth} \approx 5$ and $Re_{*rough} \approx 70$. [21] reviewed the data for a variety of roughness types and concluded that k_s/k was independent of Re_* when $Re_* \geq 80$, although 70 has been cited [24] (Figure 8).

When a surface is hydrodynamically smooth the bed shear stress is entirely viscous and $\Delta u^+ = 0$ (see eqn. (4)). Flow near a rough boundary may generate coherent flow structures similar to those in smooth boundaries. However, their shape and size are altered during the enhanced momentum exchange between the near-wall and outer flow regions [36]. This, in turn, depends on the roughness

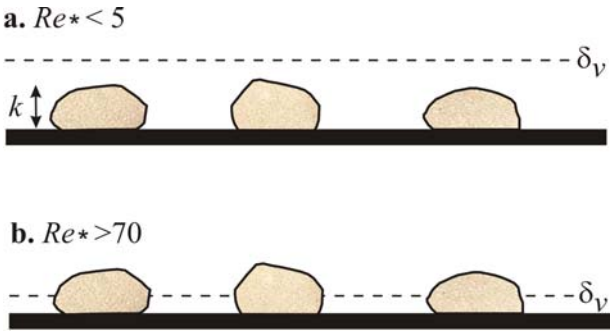

Figure 8: (a) Hydrodynamically smooth flow where $Re_* < 5$ and roughness elements are contained within δ_v, and (b) hydrodynamically rough flow where $Re_* > 70$ and roughness elements extend beyond δ_v.

geometry and configuration [25]. Sufficiently large roughness elements destroy the autonomous burst-sweep cycle characteristic of smooth boundaries, often generating more disrupted or disorganized structures that take over the role of generating turbulence at the wall [4] [13]. Turbulent structures generated by individual roughness elements provide an additional source of turbulent kinetic energy ($TKE = 1/2\left(\overline{(u')^2} + \overline{(v')^2} + \overline{(w')^2}\right)$, where $u = \bar{u} + u'$, i.e., instantaneous u = mean u + fluctuation from the mean, similarly for the other velocity components), which enhance turbulent mixing in the near wall region. Therefore, hydraulically rough flows are dominated by form drag on the roughness elements, i.e., velocity is independent of viscosity [41].

During the transition from hydrodynamically smooth to hydrodynamically rough regimes both skin and form drag are significant. Initially extra form drag is generated, which weakens the burst-sweep cycle, thus decreasing skin friction. As Re_* increases, the burst-sweep cycle becomes increasingly disrupted until it is destroyed, and the reduction in skin friction is lost, leading to an overall increase in drag. Different surfaces have different balances of both effects. [21] stated that for surfaces with sparsely distributed elements, the form drag increases before the burst-sweep cycle is modified and the reduction in skin drag is never realized. On this basis, uniformly rough surfaces are likely to be most effective for drag-reducing roughness. In the fully rough regime, Re_* is given by

$$\Delta u^+ = \frac{1}{\kappa} \ln Re_* + B - 8.5 \qquad (11)$$

and B is the smooth-wall log-law intercept equal to 5.60 [38] (see eqn. (3)). The relationship among Δu^+, Re_*, and k has been obtained experimentally for a

variety of rough surfaces in atmospheric research (review in [14]), however, no equivalent data exist for aquatic systems.

3.3 2D Transverse Bar Roughness

3.3.1 Spatial Flow Variation

Whereas the precise length scales and flow conditions vary among studies, a general pattern of the spatial variation in flow and turbulence structure over 2D transverse bars has emerged. Flow separation occurs in the lee of the roughness elements and generates a well-defined recirculation zone. Downstream vorticity is small within the separation zone in the lee of each bar. Conversely, intense vorticity is created at the height of the roughness crests due to the generation of a shear layer between the outer flow and the recirculation cell. Shear layer vortices are intensified by vortex stretching due to the high strain generated at the crest of the bars. Consequently, this region is responsible for most of the production and dissipation of TKE [4]. Under isolated roughness flow (see Figure 5a) reattachment occurs within the cavity (or jaw space, j) between adjacent elements before flow streamlines are oriented upwards as the next element is approached. In addition to the shear layer extending from each roughness crest, secondary vortices of opposing directions can form at the corners of the element, although this is dependent upon the angularity of the roughness elements.

Comparisons of the TKE production and dissipation revealed that the roughness layer over 2D transverse bars is far from an equilibrium state. Dissipation is maximized at the position of the crests due to the intensity of the vorticity associated with shear layer formation, although the maximum vorticity is smaller compared with a smooth bed. Conversely, the roughness induces an increase in the maximum production rate.

3.3.2 The Role of Roughness Geometry

The manner in which the shear layers generated over each roughness crest interacts with the roughness elements themselves is not trivial [13]. The vertical length scale of the vortices generated at the shear layers approximates k, and consequently it is reasonable to assume they dominate flow in this region. The importance of roughness index (λ/k, see Table 1) on near bed flow structure was

first noted by [29] primarily due to its impact on shear layer interaction. In addition, z_r increased with the transverse dimension of roughness elements [37]. A consideration of other parameters (e.g., shape) is also relevant (see sections 3.3.5 and 3.4).

The thickness of the roughness layer was a product of both k and d in measurements of downstream turbulence intensity, *TI,* over k-type 2D transverse square bars performed by [36]. Planar laser-induced fluorescence was used by [13] to evaluate the differences in near-bed mean flow over 2D square bar roughness where λ/k = 8 and 16. Both cases showed flow separation from the downstream edge of the roughness elements and a well-defined recirculation in its lee. The extent of this region varied between cases as flow reattachment occurred at ~ 3.5k and 4.2k for λ/k = 8 and 16, respectively. In general, the two cases exhibited similar mean flow characteristics despite the difference in λ/k, and matched the direct numerical simulation (DNS) results of [20] [25] derived using similar λ/k ratios. An examination of *TI* and Reynolds shear stress suggested that when λ/k = 16 higher downstream and vertical *TI* and Reynolds shear stress were generated in the upper 90% of flow compared to λ/k = 8, but the values remained the same near the bed.

The roughness function, Δu^+ (see eqn. (11)), can be considered a measure of the capacity of the rough surface to absorb momentum [36]. There is sufficient evidence to suggest that Δu^+ is a function of λ/k. For example, [13] showed that for λ/k = 8 and 16, Δu^+ diminished from 13.3 to 12.9, respectively and [25] used DNS to determine equivalent values of 12.0 and 11.3. A wider array of λ/k was used by [16] who found similar values at the same roughness indices. More importantly, they found that Δu^+ was maximized at λ/k = 8 and that beyond this threshold λ/k led to a decline in Δu^+. [13] demonstrated that peak turbulence production at λ/k = 16 was 14% higher than at λ/k = 8, and suggested that this represented the reduction of viscous effects in the former case. The precise mechanisms that result in deviations from the mean flow properties on either side of λ/k = 8 can be described as wake interference flow (see Figure 5b). Put simply, viscous drag and form drag combine to maximize resistance over 2D transverse roughness in turbulent flows when λ/k = 8 [24] [25].

A comparison of flow data taken over 2D transverse bars revealed that skimming flow (λ/k = 2; [26]) generated far less form drag, due to the limited connectivity between the fluid between the bars and the outer flow, than isolated roughness flow (λ/k = 11; [13]) (see Figure 5a and c). Recirculation existed across the

cavity at low λ/k and was only partly destroyed by intermittent ejections into the outer flow (see also [35]). At higher λ/k, the recirculation zone was found immediately next to each bar and was intermittent due to repeated disruption from shear layers generated at the upstream crest, which increased the connectivity between the interfacial cavities and the flow above, in particular the wake-dominated roughness layer. This suggests that the mechanism(s) of near-bed turbulence production differ between *d*-type and *k*-type roughness. In fact, low speed vortical streaks characteristic of smooth walls were observed when $\lambda/k = 2$, but were absent for $\lambda/k > 11$ [26]. *d*-type roughness and smooth beds may be more similar hydrodynamically than *d*-type and *k*-type roughness.

The effect of λ/k over 2D square bars was examined by [39] using two-equation Reynolds-Averaged Navier-Stokes (RANS) numerical modelling. They maintained a constant $k/d = 0.1$, characteristic of individual roughness elements [21] (see section 3.3.3). The roughness index varied between *d*-type and *k*-type roughness ($5 \leq \lambda/k \geq 30$) and the resistance was measured by the Darcy-Weisbach friction factor, *f*,

$$f = \frac{8\tau_w}{\rho u^2}, \tag{12}$$

which rose and fell around $\lambda/k \sim 8.8$ at a range of turbulent *Re*. They used profiles of the spatially-averaged downstream velocity to determine the 'virtual origin', or height to which the space-averaged downstream velocity vanished. The virtual origin was inversely related to λ/k, and maintained an approximately logarithmic decrease until $\lambda/k \sim 15$, whereupon it declined asymptotically. More importantly, they showed that Δu^+ was related to λ/k in a similar manner to *f*. This may explain the apparent contradiction between studies that have shown that Δu^+ both declined [13] [25] [16] and increased [26] with increased λ/k.

3.3.3 The Role of Relative Depth

Whereas there is compelling evidence that λ/k is an important parameter dictating near-bed flow structure, the difference in scale between roughness length scale and the largest turbulence scales may explain the differences between a range of studies, regardless of roughness configuration [21]. The relative height, δ/k (or blockage ratio, k/δ), provide an alternative parameter that can be used to examine whether boundary roughness affects the near bed flow. A recent review

suggested that, on average, the transition for individual roughness elements occurs when $k/\delta \leq 50$ (or $\delta/k \leq 0.02$) [21].

The relative height of the roughness elements may also influence the evaluation of the similarity hypothesis over 2D transverse bars. The results of studies from channel flows bounded on two sides [23] with regular, square bar *k*-type roughness [25] [26] and boundary layer flows with 2D transverse bars of uneven height [20], and square bars [36] (details below) showed that the outer region was significantly affected by the rough boundary. In each case, k/d was between $0.1d$ and $0.2d$, well above the threshold of $0.02d$ for transition to individual roughness elements. The effect of variable relative roughness of 2D square bars on resistance, f, and Δu^+, in fully turbulent and hydrodynamically rough flows was examined by [39] where the magnitude of resistance, f, increased with k/d across all roughness index values. Moreover, resistance became independent of Re earlier as height increased, but the flow depth had no influence on Δu^+ or the virtual origin at all Re and λ/k. In other words, flow depth had no influence on the height to which the roughness elements influenced the flow, which was in the range $0.025 < k/\delta > 0.1$, i.e., above the threshold specified above. Note that this pertains only to fully turbulent, hydrodynamically rough conditions.

DNS simulated fully-turbulent flows in a bounded channel flow with smooth and rough boundaries comprised of 2D transverse bars were examined by [4] at a much lower relative depth. The relevant geometrical parameters in the rough bed case were $k/d = 0.07$, $\lambda/k = 7$ and $Re_* = 395$. They showed that higher vorticity was exhibited within the roughness layer, that there was less Reynolds stress anisotrophy, and that structures typical of smooth boundaries became disrupted [4]. The transverse vortices were disorganized at the boundary but became increasingly coherent and organized with height until they equalled the size and intensity of those over the smooth bed, although the outer layer was unaffected. This implies that, providing mean shear is sufficient, similar structures to smooth beds will be formed, albeit away from the boundary, when relative roughness is sufficiently low. Third-order velocity moments, which are sensitive to variations in turbulent transport processes due to their high degree of non-linearity, showed that the rough bed substantially increased the transport of kinetic energy towards the boundary, but reduced it at the edge of the roughness layer. In the outer region, the smooth and rough bed cases exhibited similar characteristics. The results provide strong support for the similarity hypothesis.

3.3.4 The Importance of Reynolds Number

Experimental and modelled data from flows over 2D transverse bars at Re_* spanning transitional (Re_* = 63) and fully rough (Re_* = 121) hydrodynamic conditions were examined by [24]. Three key differences were noted: (1) the total flow resistance for transitional flow was influenced by viscous and form drag, but the viscous forces were negligible for hydrodynamically rough conditions; (2) this leads to greater coherence in near-wall structures in transitional flows; and (3) the influence of roughness on Δu^+ was less pronounced for transitional cases. Similarly, [39] determined that the effect of *Re* on *f* decreased with increasing *Re*, and *Re* independence occurred above a threshold value dictated by λ/k. The roughness function increased with Re_* across *d*-type and *k*-type roughness, ultimately exhibiting a logarithmic relationship above a threshold *Re*. At this point, the slope of the relationship recovered to κ^{-1} at sufficiently high Re_*. This facilitated the calculation of equivalent roughness height, k_s, for each bar arrangement because the relationship paralleled the correlation for sand-grain roughness (i.e., [40]). Overall, the results show that once $Re_* > 500$ the flow becomes independent of *Re*.

The precise mechanisms to account for relationships between *f*, Δu^+ and flow and roughness parameters remain uncertain. However, some insight is provided by [36] who examined turbulence structure in some detail across a range of hydrodynamically rough conditions ($30 \leq d \geq 95$ mm; $6{,}000 \leq Re \geq 48{,}450$; $355 \leq Re_* \geq 515$) over 2D transverse bars of fixed geometry (6.4 mm height and width spaced at λ/k = 8). They used quadrant decomposition to provide information regarding the turbulence structure in the near-bed region (i.e., turbulent events were sorted into quadrants of the *u′*, *w′ plane* (where *u'* and *w'* are fluctuations from the mean *u* and *w*, respectively) associated with ejections (*Q*2; $u'w' < 0$ with $u' < 0$) and sweeps (*Q*4; $u'w' < 0$ with $w' < 0$)) (Figure 9). The influence of the roughness elements on the spatial variability in time-averaged velocities was similar across all flow conditions. Upstream of each element *u* decreased and *w* increased relative to the mean values, leading to dominant *Q*2 activity. *Q*1 events dominated above the roughness element because of the acceleration in *u*, and *w* became negative downstream of the element resulting in *Q*4 dominance. As the subsequent bar is approached, the flow decelerated, leading to *Q*3 dominance. The sequence of quadrant dominance – clockwise through *Q*2-*Q*1-*Q*4-*Q*3 – is typical of surfaces where roughness

elements behave individually and flow reattachment occurs (e.g., '*k*-type' roughness; isolated roughness flow; where $\lambda/k \geq 8$). Through the use of two

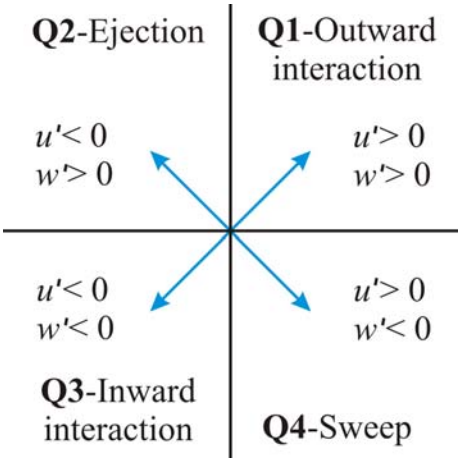

Figure 9. Quadrants are defined by the joint distribution of the velocity fluctuations from the mean downstream (u') and vertical (w') velocity components.

heights within and two heights above the roughness layer, they showed that the influence of the roughness elements on the spatial variability in time-averaged velocities declined with distance from the boundary. However, the sequence remained the same at all heights.

The form-induced stress, defined as the covariance of the spatial variation in u and w, peaked close to $z/k = 1$ and constituted 15% of τ_w. The stress rapidly declined above this height as the flow adjusted via local momentum transfer due to local imbalances in momentum and stress components [36]. This indicates that the form-induced variations in velocity disturbances were far greater in the vertical extent than the form-induced variations in stress, and that velocity disturbances may be found where stress disturbances do not exist. This results in alternating regions of upwards and downwards time-averaged form-induced momentum flux, which is particularly relevant to scalar transport and dispersion in the roughness layer [36].

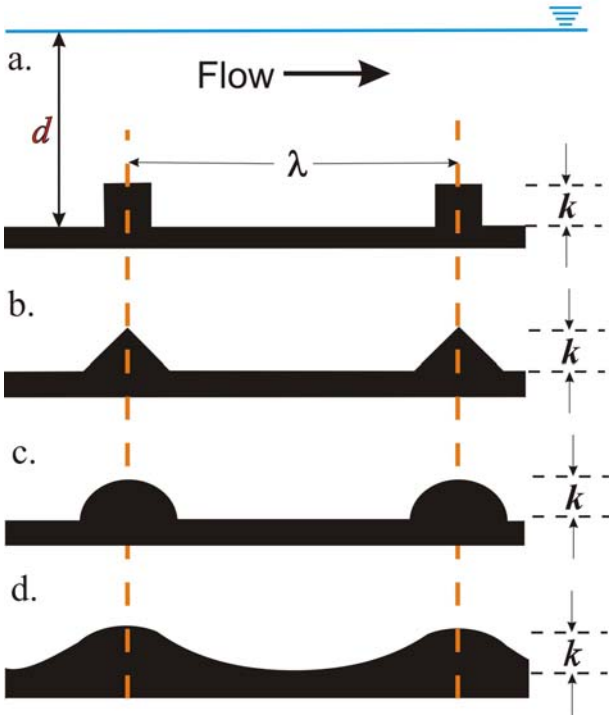

Figure 10. Schematic of channels roughened using 2D transverse bars: (a) square bars; (b) triangular bars; (c) semicircular bars; and (d) wavy wall (after [39]).

3.3.5 The Importance of 2D Transverse Bar Shape

The majority of studies of flow over 2D transverse bars have concentrated on square bars, and to a lesser extent on circular or semi-circular 'rod' roughness. However, as mentioned above, [39] used RANS modelling to examine the effect of differently shaped transverse bars (square, triangular and semicircular transverse bars, and a wavy wall) on near-bed flow structure (Figure 10). They maintained a constant relative roughness, $k/d = 0.1$, varied the roughness index to span *d*- and *k*-type roughness ($5 \leq \lambda/k \geq 30$) and used a range of Re_* and boundary layer *Re* ($Re_\delta = U\delta/\nu$). The bottom of the velocity profile (i.e., virtual origin) was displaced by ~0.8*d* (0.83*d* square bar, 0.81*d* triangular bar, and 0.79*d* semicircular bar and less so by the wavy wall condition 0.68*d*). The profiles exhibited a logarithmic region, with the exception of the wavy wall at high *Re*,

and the effective roughness height, k_s, extended higher into the flow as *Re* was increased in all cases.

All bar shapes generated an initial increase *f* with λ/k (Figure 11). In general, the resistance was positively related to the degree of angularity, e.g., when *Re* = 20,000 the maximum resistance was at $\lambda/k \sim 8.8$ for the square bar, 7.5 for the triangular bar and 7.0 for the semicircular bar, close to the threshold of $\lambda/k = 8$ (see section 3.3.2). This was followed by a decline toward the smooth wall limit, well beyond the maximum value of $\lambda/k = 30$ examined. Interestingly, the resistance offered by the square bars dropped below that of the triangular bars where $\lambda/k < 7$. This was likely due to the onset of *d*-type or wake interference behaviour in the square bars. *d*-type behaviour has not been reported for other bar types, but may be attainable using sufficiently small values of the roughness index. In contrast, *f* in the wavy wall rose and fell around $\lambda/k \sim 8$, and exhibited a decline over $5 < \lambda/k > 30$.

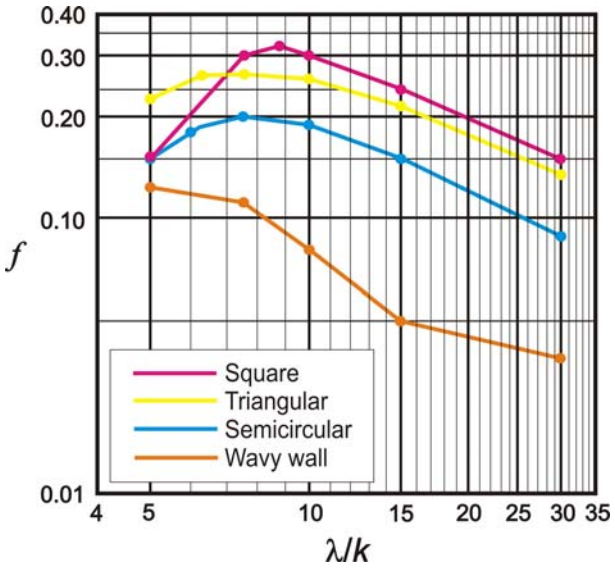

Figure 11. Mean resistance, *f*, for various bar shapes presented in Figure 10 at $k/d = 0.2$ across a range of λ/k at $Re = 10^4$ (after [39]).

The roughness function, Δu^+, was related to λ/k in a similar manner to *f*. Whereas all surfaces imparted some resistance, Δu^+ can equal zero under hydrodynamically smooth conditions, i.e., at sufficiently large λ/k. The square, triangular and semicircular bars did not exhibit $\Delta u^+ \sim 0$ across the range of λ/k

examined. However, Δu^+ of the wavy wall dropped steeply to zero (i.e., the smooth wall condition) at $\lambda/k = 30$.

The resistance over square and triangular bars increased with Re_δ before becoming independent of Re_δ. The wavy wall showed a continual decline, similar to a smooth wall but at higher values due to form drag. The semicircular bars exhibited both a rise and fall around a peak. The behaviours in the latter two cases resulted from the movement of separation and reattachment points on the curved surface [39].

As λ/k increased, form-induced stresses declined and the near-bed velocity values decreased. Whereas the shape of the bar was unimportant, the height of the bottom of the profile was inversely related to Re_*, until it declined asymptotically to a constant value. As would be expected for the profile, Δu^+ was a logarithmic function of Re_* with a slope of κ^{-1}. The correlation in each case differed by a constant that varied with bar shape and λ/k. In contrast, the slope for the wavy wall deviated considerably from κ^{-1}.

Overall, the changes in f and Δu^+ with λ/d and Re_* suggest that the hydrodynamics of the wavy wall were fundamentally different to the 'true bar' roughness types. In general, the angularity of the 'true bar' roughness elements was positively related to boundary resistance. The exception occurred for square bars at low λ/k due to the transition to *d*-type or wake interference flow, when triangular bars became hydrodynamically rougher. This suggests that square bars also behave differently from other bar shapes at low λ/d. Similar experiments at lower λ/d are required to determine if *d*-type roughness is induced for roughness exhibiting less acute angles. There were pronounced differences in the behaviour of flow over the 'wavy wall' compared to the other 2D roughness. This suggests that our understanding of 2D transverse bars may be useful for some applications, but more effort is needed in nature where bed roughness varies in angularity and regularity.

3.4 Three-dimensional Surfaces

It is useful to categorize 3D roughness into (1) 'Idealized' 3D roughness surfaces, as those surfaces comprising idealized blocks of specific dimensions, and (2) 'Complex' 3D roughness surfaces, where the specific geometry of individual roughness elements cannot be determined. In the latter, a single length

scale, k, can be used for characterization and a qualitative description of the surface is provided in lieu of other geometrical parameters.

3.4.1 Idealized 3D Roughness

Many of the relationships between the geometry and flow conditions addressed for 2D transverse bars have also been used for idealized 3D roughness elements. For example, [34] described the effects of 3D multi-scale roughness in boundary layers. They used discrete, regular blocks organized to establish surfaces of different roughness density, nA_e/A_t, which defined the ratio of the plan area of n roughness elements of individual area, A_e, to the total bed area, A_t. Roughness density values ranged from 0.008 – 0.125, which included the range common to coarse-grained rivers [34]. They used the equation

$$\frac{u(z)}{u_*} = \left(\frac{z}{d}\right)^n \tag{13}$$

in conjunction with downstream velocity profiles to determine n, which peaked at a roughness density of 0.1 (range = 0.005-0.23) before declining rapidly. Profiles of normalised downstream turbulence intensity ($TI = RMS_u/u$, where RMS_u is the root mean square velocity), revealed 3 distinct regions: (1) outer flow ($z/d > 0.35$) where TI decreased linearly towards the surface across all roughness densities, and behaved as a conventional outer boundary layer [34]; (2) an intermediate region $0.35 < z/d > 0.2$ that exhibited approximately constant TI, conforming to a zone of wake generation and dissipation; and (3) an inner region ($z/d < 0.2$) where TI diverged according to roughness density, and where the height of maximum TI was inversely related to the roughness density. Peak TI at the maximum roughness density occurred at 0.25 z/d and declined towards the bed. This height was considered a zone of transition between wake-dominated flow and the near-bed region.

Profiles of dimensionless turbulent energy dissipation, $\varepsilon d / u_*^3$, where ε is the turbulent energy dissipation rate given by

$$\varepsilon = 15\nu\left(\frac{du}{dx}\right)^2 \tag{14}$$

and ν is kinematic viscosity, increased from 10^{-2} W m^{-3} at the surface to 5 W m^{-3} at the bed. The changes in boundary layer structure in the inner and wake

regions are related to roughness density and can be explained in terms of the original classification in [29] (see Figure 5). Skimming flow occurred at the highest roughness densities where the flow shifted above the roughness elements as did the maximum ε (to z/d= 0.1, close to the top of the elements at z/d = 0.125). Intermediate roughness densities provided constant values of TI from the bed to z/d = 0.35, indicative of interacting wakes. A notable result in [34] was the absence of roughness effects in the outer flow region despite the high relative depth (k/d = 0.125) characteristic of individual roughness elements [21]. This suggests that the transverse movement of fluid between individual 3D elements led to differences in flows over 2D vs. 3D surfaces.

[39] modelled the effects of flow over uniformly distributed square and rectangular blocks in boundary layer flow with constant relative roughness, k/d = 0.1 and where the roughness index was varied to span both d-type and k-type roughness ($5 \leq \lambda/k \geq 30$). Note that no attempt was made to account for the variation in block size, and that the effective frontal blockage for the rectangular blocks was double that for square blocks. Flow was examined around (1) in-line roughness elements and (2) staggered roughness elements, where every second row was offset so that the transverse cavity between elements was blocked by elements in the subsequent row. In general, flow in the in-line arrangement remained well organized, and flow disturbance was limited to the 'immediate neighbourhood' of the elements. Conversely, the transverse movement induced by the staggered arrangement led to intense vortical motion. Comparison of spatially-averaged downstream velocity profiles showed that the in-line blocks generated logarithmic profiles, which were better defined as Re increased and k/d decreased. The flow disturbance over staggered blocks meant the log-layer was only definable when $k/d \leq 0.05$. This described a threshold where the blocks could be considered as individual element rather than components of a roughness surface.

A comparison of the resistance, f, at k/d = 0.05 (i.e., within the roughness layer) indicated that the resistance of the square blocks was lower than rectangular blocks across $6 < \lambda/k > 18$. The results were the same for both in-line and staggered arrays, but they were opposite in the case of rectangular blocks where the in-line arrangement generated a smaller resistance than the staggered case with peak values of f approximately 2.5 times smaller. The peak in f occurred over the range $10 < \lambda/k > 15$, which was similar to 2D transverse bars (section 3.3). However, the square block and the in-line rectangular arrays showed a

lower resistance than the 2D transverse bars across all cases of λ/k. This was likely due to the reduced frontal blockage compared to the 2D transverse bars. The staggered, rectangular case generated higher resistance, which suggests that the degree of transverse deviation required for flow continuity, and the resistance imparted by vorticity in this case outweighed the reduction in blockage. The Δu^+ (eqn. 11), varied logarithmically with a slope of κ^{-1} as Re_* increased, which was also the case for 2D transverse bars (see section 3.3).

3.4.2 Complex 3D Roughness

The surface characteristics of complex 3D roughness appear to explain the divergence of turbulent statistics both within and outside of the roughness layer. It is difficult to synthesize the data even when surfaces are similar, as experiments involved different: (1) measurement methods; (2) parameter calculation; (3) emphasis on different turbulent quantities; and (4) flow conditions. For example, closely packed spheres (e.g., [27]), sandpaper and sanded surfaces [15] had little effect on the outer flow. Other roughness types, such as 3D woven mesh, have been used to both support [15] and dispute [22] the concept of wall similarity.

Unfortunately, complex 3D surfaces do not lend themselves to the measurement of element spacing, not least because parameterization would need to incorporate downstream and transverse effects. Consequently, the parameterization of an irregular 3D roughness is not trivial. However, [41] examined the effect of changing Re_* on turbulence within a boundary layer over a surface with bi-directional scratches in a diamond shaped pattern for $2{,}175 < Re < 27{,}080$. The flow was in the hydrodynamically smooth and transitionally rough range ($2.3 \leq Re_* \geq 26$) given the small roughness height (k = 193 μm; k/d = 0.0025). Measurements were also taken over a smooth surface at smooth and transitional Re (Re = 3,110 and 13,140, respectively), facilitating comparison with the rough surface.

A range of turbulence statistics presented for each value of Re_* revealed the relative importance of boundary roughness on the roughness layer and outer flow region. For example, profiles of the downstream Reynolds normal stress, $\overline{u'^2}$, for $Re_* \leq 9.2$ showed no discrepancy with the smooth bed condition. As Re_* increased, however, there was a rise in $\overline{u'^2}$ in the roughness layer, and the rate at which it increased declined until $Re_* = 26$. The absence of a near-wall rise in

$\overline{u'^2}$ provided a sensitive indicator of the boundary layer reaching the fully-rough regime [27]. It represented the eventual break-up of downstream vortices generated through the burst-sweep cycle over smooth boundaries. When this occurred, the skin friction was dominated by form drag and viscous effects were negligible close to the wall. Hence, their data showed a much lower threshold value for the transition to hydrodynamically rough conditions than cited by [21] ($Re_{*rough} \geq 80$) and [24] ($Re_{*rough} \geq 70$). Moreover, [27] showed that the roughness types and uniformity dictated the threshold values. Their rough surface, consisting of uniform closely packed spheres, displayed a narrow transitionally-rough regime with $Re_{*smooth} \approx 15$ and $Re_{*rough} \approx 55$. Less uniform close packed sand grains had a wider transitionally rough regime where $Re_{*smooth} \approx 5$ and $Re_{*rough} \approx 70$. This indicates the importance of the type of roughness surface.

The effect of roughness on vertical or 'active' turbulent motions has been the topic of considerable debate. For example, vertical active turbulence is more sensitive to roughness geometry than the downstream component [13]. Profiles presented by [41] of vertical Reynolds normal stress, $\overline{w'^2}$, exhibited no difference between rough and smooth-bed cases at the full range of Re_* cited above, and maximum values were found in the log-layer. Similarly, their profiles of Reynolds shear stress, $-\overline{\rho u'w'}$, exhibited no significant changes between cases. Similarly, [37] concluded that there was similarity in $\overline{w'^2}$ outside the roughness (or viscous) layer for rough and smooth walls. Results over complex 3D surfaces do not support the similarity hypothesis. For example, [22] and [37] observed distinct differences in mean velocity and turbulent stresses in the outer region over wire mesh, and [42] stated that surface roughness had an unambiguous effect in enhancing *TI* and Reynolds shear stress over most of the boundary layer over wire mesh of a similar height. These differences are indicative of changes in the turbulent structures generated by each boundary.

Quadrant analysis (see Figure 9) was used by [41] to establish the relative contribution of individual quadrants to $-\overline{\rho u'w'}$ over smooth and rough surfaces. The contribution of $Q2$ (ejection) and $Q4$ (sweep) events to $-\overline{\rho u'w'}$ was consistent between smooth and rough-bed cases. Similar findings were made by [15] over sandpaper and woven mesh roughness, and [17] showed that sweeps and ejections occurred over rounded pebbles (k = 9 mm) regardless of boundary condition. Ejections were often coherent and identifiable within the outer flow but sweeps were confined closer to the bed, and the source of fluid for ejections in the rough case was the low-momentum fluid within cavities between

roughness elements [17]. Strong contributions to Reynolds shear stress by each quadrant were isolated by [41] who revealed that, whereas the outer flow exhibited similar contributions between smooth and rough bed cases, there was an increase in $Q4$ and a decrease in $Q2$ in the inner flow region ($y/\delta \leq 0.025$) as Re_* increased. This indicated that near the rough boundary, strong sweeps dominate over ejections in terms of their contribution to $-\overline{\rho u'w'}$. In flow over glass beads, the sweep to ejection ratio increased with roughness and high-magnitude, low-frequency events, dominating momentum transfer, increased with roughness [30]. In contrast, [22] and [37] observed a significant increase in $Q2$ contributions, and a smaller increase in $Q4$ contributions, across much of the boundary layer. The time between successive $Q2$ or $Q4$ events also increased, contradicting earlier assertions that roughness does not influence timing between quadrant events.

Ultimately, broad conclusions regarding the effects of roughness geometry and flow condition over complex 3D boundaries are limited, because of differences among studies. For example, in terms of Re_*, [22] and [37] studied flow at Re_* = 340 in the hydrodynamically rough range, which was well above the maximum Re_* = 26 used by [41] who used relative roughness, k/δ = 0.0025 (δ was substituted for d to account for differences in flow conditions), which was well below the threshold of 0.02 for the transition to 'individual roughness elements' cited by [21]. Both [22] and [37] used k/δ = 0.066 (woven mesh), and suggested that each wire behaved independently, whereas [15] used k/δ = 0.016 (sandpaper) and k/δ = 0.022 (woven mesh), which would be in the 'transitional' range (i.e., k/δ > 0.0125 or 0.025) for outer-region similarity [21]. In [42] k/δ = 0.016 (wire mesh) and flow was below the hydrodynamic rough threshold (Re_* = 17). Flow over an array of roughness geometries (sand, variously sized and spaced spheres, hemispheres and fences) may provide the same effect on the mean downstream velocity profile, although mechanisms of turbulence generation, mixing and dissipation may differ [40]. Unfortunately, few direct comparisons can be made between studies to isolate the specific effects of 3D roughness type. However, [42] were able to isolate the effects of a smooth surface, a grain roughness ($k = D_{50}$ = 1.2 mm) and a wire mesh (k = 0.6 mm) on turbulence structure by maintaining an approximately constant Re (u and d constant). Their data can be augmented by [37] who used wire mesh of k = 0.69 mm under similar flow conditions. In each case, the rough surfaces increased Δu^+ and downstream TI increased at all heights relative to a smooth

surface. Profiles of the vertical *TI* on rough surfaces were higher than the smooth-wall data, likely because the surface roughness was substantial for the wire mesh data, but only marginal for sand grains. As mentioned above, surface roughness has a stronger effect on the vertical than downstream *TI* [23], and [42] demonstrated that the effects of surface roughness on $\overline{-\rho u'w'}/U$ were more distinct in the roughness layer.

The grain roughness increased peak *TI* values, which were located at $z/d = 0.08$, by ~20% compared to the smooth boundary. The mesh roughness caused an increase of ~40%, and the peak was located at $z/d = 0.09$, which was similar to peak values at $z/d = 0.04$ found by [37]. Although the wire diameters were only about 50% of the nominal height of the sand grains, the wire mesh data had significantly higher *TI* and Reynolds shear stress values. This further indicates that the effects of 3D roughness geometry and spacing are more than simply a function of k.

4.0 Summary and Key Findings

Whereas much has been learned about flow over rough boundaries, much of the environmental hydraulics of natural systems remains to be examined. This is due to several factors including: (1) the emphasis on mean effects rather than detailed structure of the flow; (2) the use of different parameters to examine turbulence; (3) the difficulty in finding a standard parameterization for a wide variety of roughness surfaces, particularly complex 3D roughness; and (4) the difficulty in comparing data from different measurement techniques. This has led to conflicting results in some cases and lack of clearly defined trends in others. Despite these issues, the following conclusions can be drawn:

- **The height to which the roughness layer extends, z_r ,** is generally found within the range $2 < k > 5$. However, some examples indicate it may be as high as $8k$ due in part to the precise geometry of the surface, and the way in which z_r is determined (e.g., location of the maximum Reynolds shear stress, third-order velocity statistics).
- **The roughness Reynolds number, $Re_* = u_* k/\nu$,** is a fundamental parameter that describes the balance between viscous and form drag forces imparted by boundary roughness. *Hydrodynamically rough flow*s occur at high values of Re_* and represents the dominance of form drag induced by the generation of TKE around roughness elements, where velocity is independent of viscosity.

Under *hydrodynamically smooth conditions* the boundary shear stress (τ_w) is largely viscous and velocity is governed by viscous forces. Under *transitionally rough flows* both viscous and form drag dictate near-bed velocity and turbulence production. An increase in Re_* will disrupt the burst-sweep cycle inherent to viscous forces and promote form drag.

- There is little consensus on how to determine the **transition threshold between hydrodynamically smooth and rough flows** because the use of simple measures such as k neglect the effects of other geometrical parameters such as spacing, shape and 2D vs. 3D dimensionality. The transition has been reported to occur between $Re_{*smooth} \approx 15$ and $Re_{*rough} \approx 55$ for uniform close-packed spheres, and between $Re_{*smooth} \approx 5$ and $Re_{*rough} \approx 70$ for less uniform close packed sand grains. These latter values have been supported by an evaluation of flow over a variety of roughness types, which found that k_s/k becomes independent of Re_* when $Re_* \geq 70 - 80$.
- **The ratio of the spacing between roughness elements and roughness height**, $\boldsymbol{\lambda/k}$**,** is a geometrical parameter that dictates the influence of boundary roughness on the roughness layer. A number of non-dimensional indices have been used to evaluate roughness (e.g., roughness index, λ/k; relative roughness spacing, k/λ; and dimensionless groove width, j/k; Table 1) over 2D transverse bars.
- **The effect of** $\boldsymbol{\lambda/k}$ is well understood due to the focus on the effects of spacing between roughness elements for 2D transverse bars, in part due to the ease of measuring and changing geometrical parameters in 2D cases. For flows with $\boldsymbol{\lambda/k < 8}$ the connectivity between the fluid in the space between roughness elements and the flow above becomes increasingly limited (i.e., *skimming flow*; *d*-type roughness). For flows with $\boldsymbol{\lambda/k \sim 8}$ the turbulent wakes generated around individual roughness elements interact the most (i.e., *wake interference flow*), minimizing viscous drag but maximizing form drag. For flows with $\boldsymbol{\lambda/k > 8}$ the interaction of wakes decreases towards *isolated roughness flow*, where the recirculation within the interfacial sublayer is intermittent and limited to the zone in the immediate lee of individual roughness elements.
- **The roughness function,** $\boldsymbol{\Delta u^+}$, is a measure of the capacity of the rough surface to absorb momentum (i.e., a surrogate measure of resistance) and is related to k. It can be calculated from the dimensionless law-of-the-wall (eqn. 3). Where $\lambda/k < 8$, Δu^+ increases with λ/k, because turbulence

production is lowered by the viscous forces in the near-bed region. Where $\lambda/k \geq 8$, Δu^+ decreases with λ/k, because viscous forces are reduced and turbulence production is higher, generating a larger sink for momentum.

- **The relative height, δ/k, or blockage ratio, k/δ**, can be used to determine whether boundary roughness can be considered as a single roughness surface or as one containing multiple, individual roughness elements. Variations in these parameters may be related to the contradictory statements regarding the similarity hypothesis. However, there is no threshold that can be applied to all surfaces given the influence of other geometrical parameters. A recent review suggested that, on average, individual roughness elements exist when $\delta/k \leq 50$ (or $k/\delta \geq 0.02$).
- **Block-like 3D surfaces** that can be parameterized in a similar manner to 2D transverse bars are better understood than those that cannot. Height is the only definable parameter, which is often insufficient for predicting turbulence in the roughness sublayer.

Whereas our knowledge of 2D systems has improved substantially, the application of this knowledge to natural systems is limited given the apparent (but as yet unclear) differences in the hydrodynamics of 3D systems. Ultimately, systematic investigations of flow over complex, 3D surfaces are required, and should incorporate: (1) hydrodynamically smooth, transitional and rough flows; (2) a range of relative depths, k/d, to establish the thresholds at which roughness elements start to behave 'individually' over different surfaces; and (3) a greater emphasis on the transverse flow component. Such a framework requires that a universal method of parameterizing 3D roughness geometry be developed, possibly from existing statistical or numerical modelling methods.

APPENDIX- LIST OF SYMBOLS

List of *S*ymbols

Symbol	Definition	Dimensions
A_e, A_t	Area of individual roughness elements, bed area	$[L^2]$
B	Smooth-wall log-law intercept (= 5.6)	-
C_D	Drag coefficient	-
d	Flow depth	[L]

d_0	Zero plane displacement	[L]
d/k	Blockage ratio	-
D	Molecular diffusivity	[L^2 T^{-1}]
D_x	Percent of cumulative grain size distribution	-
f	Darcy-Weisbach friction factor	-
H_x *or* H_y	Scaling exponent	-
j	Groove width	[L]
k, k_s	Roughness height, Equivalent roughness height	[L]
k/d or k/δ	Relative roughness	-
K_3	Max difference between 3 adjacent points on a bed	[L]
l	Downstream length of roughness element; length scale	[L]
n	Number of elements in a cross-section	-
P	Wetted perimeter	[L]
Re, Re_*, Re_x, Re_δ	Reynolds number, Roughness Re, Local Re, Boundary Layer Re	-
TI	Turbulence intensity	-
TKE	Turbulent kinetic energy	[L^2 T^{-2}]
U, U_0	Mean downstream velocity, free stream velocity	[L T^{-1}]
u_s	Instantaneous surface velocity	[L T^{-1}]
u , v , w	Instantaneous velocity in x, y, and z directions	[L T^{-1}]
u' , v' , w'	Deviation from mean velocity in x, y, and z	[L T^{-1}]
u_*	Friction velocity	[L T^{-1}]
u^+	Dimensionless downstream velocity	-
$\overline{u'^2}$, $\overline{v'^2}$, $\overline{w'^2}$	Reynolds normal stress in x, y, and z directions	[L^2T^{-2}]
x , y , z	Downstream, transverse, and vertical distance	[L]
z^+	Dimensionless height	-
z_0, z_R, z_L, z_c	Roughness height, height of roughness layer, height of logarithmic layer, and height of roughness crests	[L]

Δu^+	Roughness function	-
$\partial u/\partial z$	Vertical velocity gradient	$[T^{-1}]$
δ_D, δ_v, δ_I, δ_F, δ_R, δ_t	Diffusional sublayer thickness, Viscous sublayer thickness, Inertial sublayer thickness, Form-induced sublayer thickness, Roughnesss layer thickness, and Interfacial sublayer thickness	[L]
ε	Turbulent energy dissipation	$[L^2\ T^{-3}]$
σ_z	Standard deviation of bed elevations	[L]
ω	Wake function	-
Π	Wake strength	-
κ	von Kármán constant (equal to 0.4)	-
ν	Kinematic viscosity	$[L^2\ T^{-1}]$
λ	Wavelength	[L]
λ_{Crit}	Critical wavelength for wake interference flow	[L]
ρ	Density of water	$[M\ L^{-3}]$
$-\rho\overline{u'w'}$	Reynolds shear stress	$[M\ L^{-1}\ T^{-2}]$
τ_w	Bed or wall shear stress	$[M\ L^{-1}\ T^{-2}]$

Acknowledgments

This work was supported in part by funding from the Natural Sciences and Engineering Research Councils of Canada through a Discovery Grant and a Strategic Project Grant (STP 322317-05) to JDA.

References

1. J. Aberle and V. Nikora, *Water Resour. Res.* W11414 (2006).
2. J. Aberle and G.M. Smart, *J. Hydraul. Res*. 41, 259– 269 (2003).
3. J.D. Ackerman and T.M. Hoover, *Limnol. Oceanogr.* 46, 2080-2087 (2001).
4. A. Ashrafian and H.I. Andersson. *Int. J. Heat Fluid Fl.* 25, 65-79 (2006).
5. N.E. Bergeron, *Math. Geol.* 28, 537-1603 (1996).
6. B.P. Boudreau and B.P. Jørgensen, The benthic boundary layer (Oxford, 2001).

7. D.I. Bray, Flow resistance in gravel-bed rivers. R.D. Hey, J.C. Bathurst, and C.R. Thorne Eds., Wiley, 109 (1982).
8. F.H. Clauser, *J. Aeronaut. Sci*. 21, 91–108 (1954).
9. N.J. Clifford, A.R. Robert and K.S Richards, *Earth Surf. Proc. Land.* 17, 111-126 (1992).
10. J.A. Davis and L.A. Barmuta, *Freshwat. Biol.* 21, 271-282 (1989).
11. C. de Jong, *Berlin. Geogr. Abh*. 59, 1–229 (1995).
12. L. Djenidi, R. Elavarasan and R.A. Antonia, *J. Fluid Mech*. 395, 271–294 (1999).
13. L. Djenidi, R.A. Antonia, M. Amielh and F. Anselmet, *Exp Fluids* 44, 37-47 (2008).
14. J. Finnigan, *Annu. Rev. Fluid Mech.* 32, 519–71 (2000).
15. K.A Flack, M.P. Schultz and T.A. Shapiro, *Phys. Fluids* 17, 035102 (2005).
16. Y. Furuya, M. Miyata and H. Fujita, *J. Fluid. Eng.* 98, 635–644 (1976).
17. A.J. Grass, *J. Fluid Mech.* 50, 233–255 (1971).
18. F.R. Hama, *Trans. Soc. Naval Archict. Marine Eng.* 62, 333–358 (1954).
19. T.M. Hoover and J.D. Ackerman. *J. Environ. Eng. Sci.* 3, 365-378 (2004).
20. T. Ikeda and P.A. Durbin, *J. Fluid Mech*. 571, 235–263 (2007).
21. J. Jimenez, *Ann. Rev. Fluid Mech*. 36, 173–196 (2004).
22. P.A. Krogstad, R.A. Antonia and L.W.B. Browne, *J. Fluid Mech.* 245, 599–617 (1992).
23. P.A. Krogstad and R.A. Antonia, *Exp. Fluids* 27, 450–460 (1999).
24. P.A. Krogstad, H.I. Andersson, O.M. Bakken and A. Ashrafian, *J. Fluid Mech.* 530, 327–352 (2005).
25. S. Leonardi, P., Orlandi, R.J. Smalley, L. Djenidi and R.A. Antonia, *J. Fluid Mech*. 491, 229–238 (2003).
26. S. Leonardi, P. Orlandi, R.J. Smalley, L. Djenidi and R.A. *Int. J. Heat Fluid Fl.* 77, 41–57 (2004).
27. P.M. Ligrani and R.J. Moffat *J. Fluid Mech.* 162, 69–98 (1986).
28. B.J. McKeon, C.J. Swanson, M.V. Zagarola, R.J. Donnelly and A.J. Smits, *J. Fluid Mech*. 511, 41-44 (2004).
29. H.M. Morris, *Trans. Am. Soc. Civil Eng.* 120, 373-398 (1955).
30. S. Nakagawa and I. Nezu, *J. Fluid Mech.* 80, 99-128 (1977).
31. V. Nikora, D. Goring and B.J.F. Biggs, *Water Resour. Res*. 34, 517– 527 (1998).
32. V. Nikora, D. Goring, I. McEwan and G. Griffiths, *J. Fluid. Eng.* 127, 123-133 (2001).
33. G.N. Nishihara and J.D. Ackerman. Mass transport in aquatic environments. C. Gualtieri and D.T. Mihailovic Eds. Taylor & Francis, 299 (2008).
34. R. M. Nowell and M.A. Church, *J. Geophys. Res.* 84, 4816-4824 (1979).

35. A.E. Perry, W.H. Scholfield and P.N. Joubert, *J. Fluid Mech*. 165, 383-413 (1969).
36. D. Pokrajac, L.J. Campbell, V. Nikora, C. Manes and I. McEwan, *Exp. Fluids* 42, 413-423 (2007).
37. M.R. Raupach, R.A. Antonia and S. Rajagopalan, *Appl. Mech. Rev*. 44, 1–25 (1991).
38. A.R. Robert, River processes (Arnold, 2003).
39. D.N. Ryu, D.H. Choi and V.C. Patel, *Int. J. Heat Fluid Fl.* 28, 1098–1111 (2007).
40. H. Schlichting, Boundary layer theory 7th Ed (McGraw Hill 1979).
41. M.P. Schultz and K.A. Flack, *J. Fluid Mech.* 580, 381–405 (2007).
42. M.F. Tachie, D.J. Bergstrom and R. Balachander, *Exp. Fluids* 35*,* 338-346 (2003).
43. P.L. Wiberg and J.D. Smith, *Water Resour. Res.* 27, 825–838 (1991).
44. W.J. Young, *Freshwat. Biol.* 28, 383-391 (1992).